

Plasma Temperature Measurement with a Silicon Photomultiplier (SiPM)

E. D. Hunter,^{1, a)} J. Fajans,^{1, b)} N. A. Lewis,^{1, c)} A. P. Povilus,^{1, d)} C. Sierra,^{1, c)} C. So,² and D. Zimmer^{1, e)}

¹⁾*Department of Physics, University of California, Berkeley, California*

²⁾*Department of Physics and Astronomy, University of Calgary, Canada*

(Dated: 2 September 2022)

The temperature of a nonneutral plasma confined in a Penning-Malmberg trap can be determined by slowly lowering one side of the trap's electrostatic axial confinement barrier; the temperature is inferred from the rate at which particles escape the trap as a function of the barrier height. Often, the escaping particles are directed toward a microchannel plate (MCP), and the resulting amplified charge is collected on a phosphor screen. The screen is used for imaging the plasma, but can also be used as a Faraday cup FC for a temperature measurement. The sensitivity limit is then set by microphonic noise enhanced by the screen's high voltage bias. Alternately, a silicon photomultiplier (SiPM) can be employed to measure the charge via the light emitted from the phosphor screen. This decouples the signal from the microphonic noise and allows the temperature of colder and smaller plasmas to be measured than could be measured previously; this paper focusses on the advantages of a SiPM over a FC.

I. INTRODUCTION

Nonneutral plasmas (plasmas with a single sign of charge) can be confined in Penning-Malmberg traps. These traps¹ consist of a stack of cylindrical electrodes aligned parallel to a strong axial magnetic field. The magnetic field provides radial confinement for the plasma, while potentials applied to the electrodes provide axial confinement. The traps can confine electrons, positrons, antiprotons, ions, and single-sign mixtures, though we will here describe results with electrons only. Penning-Malmberg traps have been used in basic plasma physics experiments on, for instance, collision rates,^{2,3} compression,⁴ centrifugal separation,⁵ cavity cooling⁶, and electron cyclotron resonance (ECR)⁷ and magnetometry,⁸ as well as having been used to synthesize antihydrogen atoms.⁹ Determining the temperature of the confined plasmas is critical to these experiments.

For anything other than certain ions, florescent-based temperature diagnostics are not available. Instead, the most common temperature diagnostic functions by measuring how fast electrons “evaporate” as one of the side well barriers is lowered (see Fig. 1).¹⁰ More precisely, we obtain $N(E_B)$, the often microchannel-plate-(MCP)-amplified number of electrons that escape the plasma as a function of the energy barrier height $E_B(t, r)$. E_B is controlled by the time (t) dependent voltages applied to the confining electrodes as well as by the plasma's self consistent potential. It is also a function of the radius r from the trap axis. The temperature is then determined

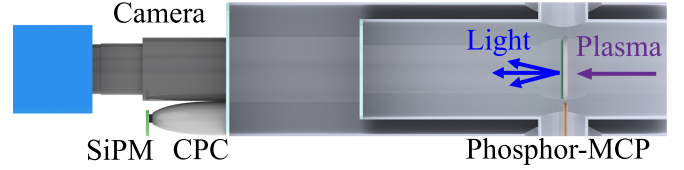


FIG. 1. Scaled schematic showing collection optics that concentrate the light signal onto the SiPM. Plasma is dumped from a trap (not shown) onto the MCP at the right. Each plasma electron produces a cascade of up to 18 000 electrons in the MCP. These electrons are accelerated onto a fast phosphor (P47) to produce blue photons. The plasma signal can be read via the light produced (SiPM) or the charge on the phosphor screen (FC). A CCD camera is used to determine the plasma radial density profile.

by fitting the rising edge of the signal, $N(E_B)$, to an exponential of the form $\exp[-E_B(t, r)/k_B T]$, where k_B is Boltzmann's constant, and T is the temperature.^{10,11}

The exponential form of $N(E_B)$ results from the assumed Maxwellian distribution of the plasma electrons, and is only valid for electrons that come from the high-energy tail of the distribution. The particles near the axis face a lower energy barrier, and escape first. As ever more electrons escape, the self-consistent plasma potential begins to change. The self-consistent barrier height E_B becomes increasingly dependent on $N(E_B)$, and $N(E_B)$ itself becomes independent of the temperature. Effectively, only electrons that escape from the inner radial core of the plasma contain temperature information.^{10,11} This core, roughly confined within a Debye radius of the trap axis, contains $\sim \pi \epsilon_0 k_B T L_p / q^2$ electrons, where L_p is the plasma length and q is the electron charge. Notably, the number of electrons in the core is independent of the plasma density, and at low temperatures, this number is not large. For instance, for a plasma with $T = 10$ K and $L_p = 5$ mm, fewer than 1000 electrons contain significant temperature information. A sensitivity approaching one electron charge is necessary to measure the temperatures of plasmas with such parameters.

Traditionally, $N(E_B)$ was collected using the phosphor

^{a)}eric.hunter@berkeley.edu; Permanent address: Stefan Meyer Institute for Subatomic Physics, Vienna, Austria

^{b)}joel@physics.berkeley.edu

^{c)}Permanent address: Department of Physics, University of Michigan, Ann Arbor, Michigan

^{d)}Permanent address: Lawrence Livermore National Laboratory, Livermore, California

^{e)}Permanent address: Department of Mechanical and Aerospace Engineering, University of California, San Diego, California

screen as a Faraday cup (FC). The screen must be biased to a voltage higher than the accelerating voltages employed by the MCP: typically, a minimum of ~ 1 kV. If the screen is simultaneously used for imaging, the bias must be increased to 4.5 kV or above, since the electrons require 1–2 keV to penetrate the aluminium coating on the screen. The signal, $N(E_B)$, comes from a capacitive pickoff on the screen bias circuitry. The high bias voltage on the screen enhances the microphonic noise inevitably present on the pickoff. The background environmental vibrations that induce this noise are strongly enhanced by the proximity of the active cooling systems associated with the magnet and cryogenic plasma trap. Even without such cooling systems, microphonic noise dominates over electronic noise in the system.

The technique presented in this paper bypasses the bias coupling by using the blue light emitted from the P47 phosphor screen as a proxy for the incident charge. This light is unaffected by the vibrations, and, hence, is immune to the microphonic noise. To obtain $N(E_B)$ from the phosphor light, we have used both traditional photomultiplier tubes and Silicon Photomultipliers (SiPM). Although photomultiplier tubes may have a lower dark count than SiPMs, they must be placed some distance away from the experiment because of the magnetic fringe field of the Penning-Malmberg trap. Even so, with extension optics they yield a superior signal compared to the signal from a Faraday cup.

In this paper, we describe light-collection results with SiPMs only because they are insensitive to the magnetic field¹² and can be placed just outside the trap vacuum window, much closer to the phosphor screen. Consequently, they can collect much more light than a photomultiplier tube, and in this application, yield equivalent results. Moreover, unlike photomultiplier tubes, SiPMs are not as delicate, are relatively inexpensive, and are not degraded by exposure to ambient light.^{13–15}

II. DETECTOR CIRCUITRY AND SENSITIVITY

1. Faraday Cup Circuit

Our FC-based diagnostic measures the plasma charge using the circuit in Fig. 2. The RC network on the right filters noise from the high-voltage power supply. The 20 nF pickoff capacitor blocks the DC bias voltage on the phosphor screen while coupling the signal to the subsequent SRS SR560 amplifier. The back-to-back diodes protect the SRS amplifier from voltage spikes when the high voltage supply is turned on and from faults. One plasma electron impinging on the MCP multiplies to ~ 18000 electrons at maximum MCP gain. These electrons are accelerated towards, and then collected on, the phosphor screen, where they induce a $\sim 2 \mu\text{V}$ signal on the 1 nF output capacitor. This charge decays through the 1 M Ω resistor.

The microphonic noise caused by vibrations of the high-voltage phosphor screen bias lead is the primary source of noise. The noise in our system is dominated by vibrations from the coldhead (Sumitomo RDK-

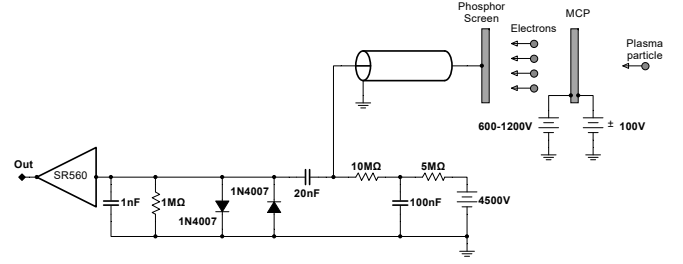


FIG. 2. Biasing circuit and AC coupled pickoff for the phosphor screen. In addition to the capacitors explicitly shown in this schematic, there is also a ~ 300 pF “parasitic” capacitance on the coax lead going to the screen.

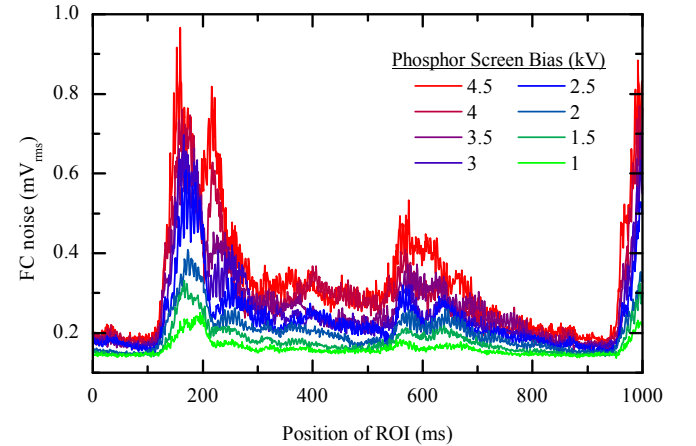


FIG. 3. FC noise due to microphonics related to the coldhead, and measured on the 1 nF capacitor in the circuit of Fig. 2 as a function of the phosphor screen bias. The RMS noise (minus DC offset) is measured for a 1 ms moving window (ROI), and averaged over 30 traces. Traces were collected with a trigger synchronous with the coldhead.

415D) that cools the electrode stack. The coldhead generates periodic noise associated with intervals of maximum and minimum vibrations. To study this effect, we created an audio trigger synchronized with the loudest part of the periodic coldhead cycle. Figure 3 displays the RMS noise in the FC signal as a function of time from this trigger. The period of elevated noise, beginning around 100 ms, persists at some level for nearly the whole trace. The noise increases as the phosphor bias is raised toward the level required for imaging (4.5 kV).

Even if the plasma temperature is measured during the FC quiet intervals, which is sometimes possible, the noise is 0.1–0.2 mV. The noise principally comes from ambient vibrations, with a component from power supply noise. For reference, the Johnson noise is about 0.002 mV, the noise from the SRS amplifier is about 0.004 mV, and the ADC noise is about 0.03 mV.

2. Faraday Cup Calibration and Signal-to-Noise Ratio

To optimize the signal-to-noise (SNR) ratio for FC-based measurements, we run the MCP at maximum gain: a front-to-back bias differential of about 1 kV. The phos-

phor screen is normally biased a few hundred volts higher than the back of the MCP in order to attract and capture all the electrons leaving the MCP while minimizing the microphonic noise.

The noise is best characterized in terms of the number of equivalent plasma electrons. This number can be estimated from the FC data in Fig. 4. This data was taken with an SR560 gain of 2, so a single plasma electron generates a signal of about 0.004 mV. The FC RMS noise level, taken before the signal starts to rise, is about 0.51 mV. Thus, the noise is equivalent to the signal from about 130 plasma electrons. Our circuit functions as an integrator with a time constant long compared to the observation time; we would expect to be able to distinguish a signal once the number of electrons that have escaped the plasma exceeds this threshold.

As can be seen in Fig. 4, the signal initially doubles over a time, corresponding to a signal frequency, in which there is significant noise variation; i.e. the signal and noise frequencies overlap. Consequently, it is not possible to greatly improve the SNR by filtering.

Across all five^{3,5,6,9,16} of the Penning-Malmberg traps that the authors have worked on, at three different institutions, microphonic noise has been the dominant noise source for FC pickups. The best noise performance has been approximately the same (within about an order of magnitude) on experiments that use an MCP^{5,6,9,16-18} or a cryogenic amplifier placed close to the FC.³ Attempts to bring a raw FC, no-MCP signal out of the vacuum chamber dramatically increase the noise. This is particularly true for cryogenic traps, as cryogenic coax cables appear to be particularly noisy.

3. Silicon Photomultiplier Circuit

We use the SensL C-Series 60035 SiPM, a solid state device constructed of 19600 cells in a 6 mm by 6 mm square, though we believe similar results would be obtained for any similar SiPM. Each cell contains one Geiger-mode photodiode and quench resistor in a parallel arrangement, resulting in a total output signal that is the sum of the entire array. The device receives a positive reverse bias at the (parallelized) cathode, which normally exceeds the reverse breakdown voltage of ~ 24.5 V by a few volts (the “overvoltage”). The gain is a sensitive function of the overvoltage. The output is taken from the anode and amplified by an ADA4898-based transimpedance amplifier. It is linearly related to the light intensity as long as 1) the voltage developed at the anode is much less than the overvoltage, a condition enforced by the transimpedance amplifier, and 2) the individual cells do not saturate from multiple photons. A simplified schematic of the SiPM circuit is shown in Fig. 5.

The primary noise source within the SiPM is the dark count rate (DCR): the rate at which thermal excitations trigger electron avalanches in the cells. The DCR increases with the cell temperature, the detector area, and the overvoltage. The overvoltage is the most readily adjustable parameter, but it also controls the gain of the SiPM. A variable bias voltage was incorporated into the

SiPM circuit to enable precise tuning of the overvoltage to achieve optimal performance.

The bias voltage is set by changing the resistance of a non-volatile digital potentiometer (AD5141) in the feedback loop of an adjustable voltage regulator (LM317L). The AD5141 is, in turn, set over the SPI bus by an Arduino microcontroller which is ultimately disconnected from the circuit. A digital potentiometer was chosen over its manual equivalent due to the former’s consistent, quiet nature and remote programmability.

The optimal bias voltage—roughly 28.5 V in our case—corresponds to the peak SNR. This value is determined by exposing the SiPM to light pulses from a blue LED and measuring the maximum amplitude response when normalized by the RMS noise.

To allow room for a CCD camera, which is used to image the plasma, the SiPM is placed off the trap’s optical axis. This decreases the amount of light collected by about a factor of two. This signal loss is compensated for by the inclusion of an acrylic compound parabolic concentrator (CPC), which concentrates light onto the SiPM. The CPC has optical grease applied to both ends and silver-coated sides to maximize internal reflections. The light gain of the CPC was measured using a digital camera and is approximately a factor of 5. In experiments not reported here, we have also used an open-center, tilted Fresnel lens to gather even more light.

4. Silicon Photomultiplier Calibration and Signal-to-Noise Ratio

For SiPM-based measurements, the phosphor screen must produce light. This requires a screen bias voltage much higher than that used for the FC-based measurements. Typically we use the same bias as for imaging the plasma: 4.5 kV or greater. The SNR is highest with the MCP gain at its maximum, and we will report the SNR under these conditions. However, we can use lower MCP gains and still measure satisfactory temperatures; this has some advantages which will be discussed later.

To determine the mean amplitude of single plasma-electron events, we slowly release a small number of electrons ($\sim 10^2$) from the plasma onto the MCP so that each arriving electron is well separated in time (see Fig. 6). Each “hit” has a sharp rise followed by an exponential decay with a time constant of about 300 ns.

Figure 7 displays the averaged pulse amplitude histogram of four 3 s samples similar to that shown in Fig. 6. The MCP gain was at its maximum, and the phosphor bias was 4.5 kV. In addition to the signal from the roughly 100 electrons per sample, this histogram includes the SiPM dark counts that occurred during the samples. With these counts subtracted, the analysis shows that the signals from the plasma electrons have a broad distribution with a mean height of about 9 mV.

Noise in our system comes primarily from dark counts in the SiPM. With our preferred SiPM overvoltage, the average Poissonian interval between counts is $1 \mu\text{s}$. This DCR is much higher than it would be if we had used a photomultiplier tube instead of a SiPM.¹³ Nonetheless, it causes few operational difficulties because the dark count

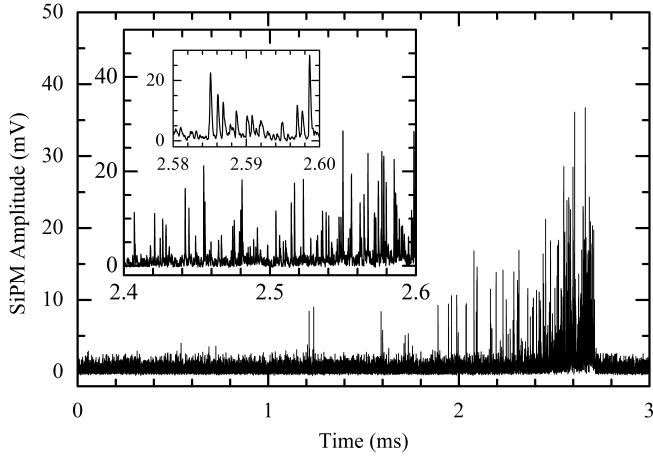


FIG. 6. Typical extraction trace for ~ 100 trapped electrons. The larger inset shows that most hits appear to be isolated even in the densest portion of the extraction. The smaller inset shows the time history of individual hits.

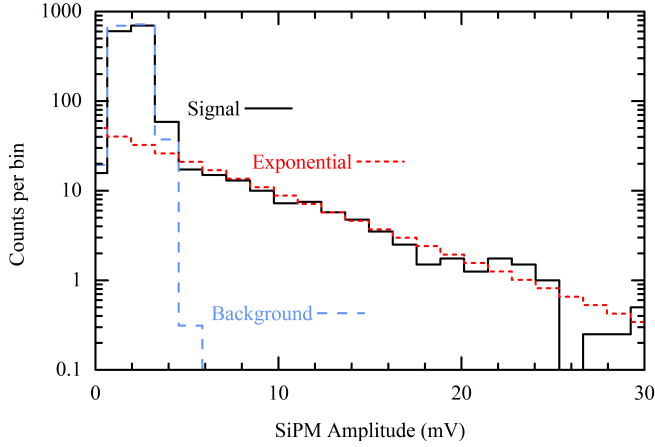


FIG. 7. Averaged pulse height distribution (black) for four ~ 100 -electron traces similar to that shown in Fig 6. The background, without any electrons, is shown in blue, and an exponential fit is displayed in red.

$\sim \pi \epsilon_0 k_B T L_p / q^2$ electrons to escape, but for these first electrons, $N(E_B)$ will increase linearly on a log scale. This log-linear regime is the focus of this paper, though slightly more information can be gained by using a more complicated fitting function that goes into the “bend-over” region at higher N .^{10,11} The data is actually fit to a slightly extended model, $a + b \exp[-E_B/k_B T]$, where a and b are nuisance parameters that allow for an offset from zero in amplitude and in time.

Since the useful range of N has an upper bound, the range of the fitting region, and hence the quality of the fit, will depend on the usable lower bound of the data. This lower bound is set by the background noise level. In Fig. 4 we compare the output of the FC and SiPM detectors at three different MCP gain settings. The traces were not acquired simultaneously as the FC and SiPM require different phosphor screen bias voltages for optimal performance. However, the six analyses shown were done on nominally identical plasmas.

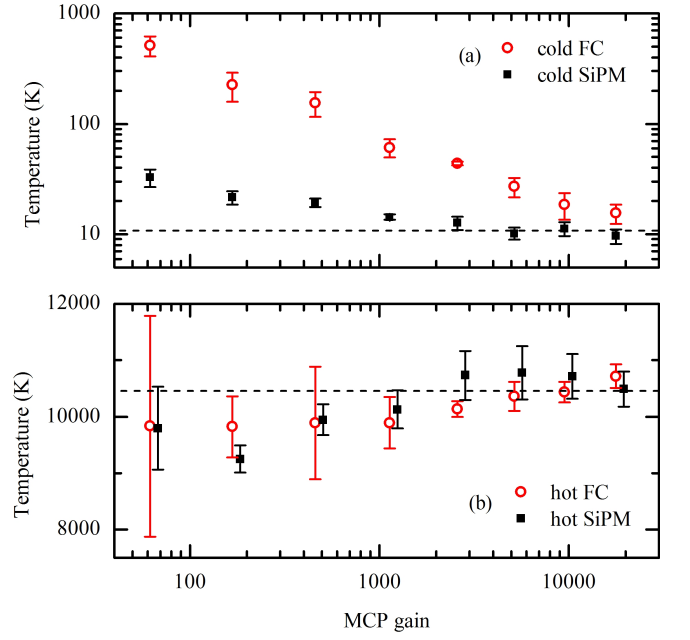


FIG. 8. Measured plasma temperature as a function of MCP gain for (a) very cold and (b) very hot plasmas. Error bars represent the standard deviation of the temperature measured in multiple trials; in (b), the SiPM points were horizontally displaced around their true center for clarity.

It is clear from the traces in Fig. 4 that the SiPM is much more sensitive than the FC at any MCP gain. While the noise floor is about the same for the SiPM and the FC, the SiPM gain is higher, so the straight line region is longer. Indeed, at these temperatures, it is difficult to unambiguously identify a straight line region in the FC data.

In Fig. 8, we show the temperatures reported for very hot and very cold plasmas as a function of MCP gain. For hot plasmas, the measured temperatures for both detectors converge to the highest MCP gain value, and are never more than about 10% from this value. For cold plasmas, the SiPM temperatures asymptote to the temperature found with the highest MCP gain, and are within about 20% for all gains above $\times 2000$. The FC temperatures asymptote towards this same value, but much more slowly, and in all cases yield higher temperatures; for lower MCP gains, the temperatures are significantly higher.

We have used the SiPM-based diagnostic to measure the temperatures of plasmas with as few as 300 trapped electrons. For fewer electrons, collisions do not necessarily adequately Maxwellianize the plasmas, particularly as the collision rate can be strongly suppressed by O’Neil’s adiabatic invariant.¹⁹

IV. PLASMA SPACE CHARGE AND SIMULTANEOUS IMAGING

With the FC, the MCP must be run at its highest gain. While the MCP is linear for the first electrons that escape, it soon saturates at this gain. With the SiPM,

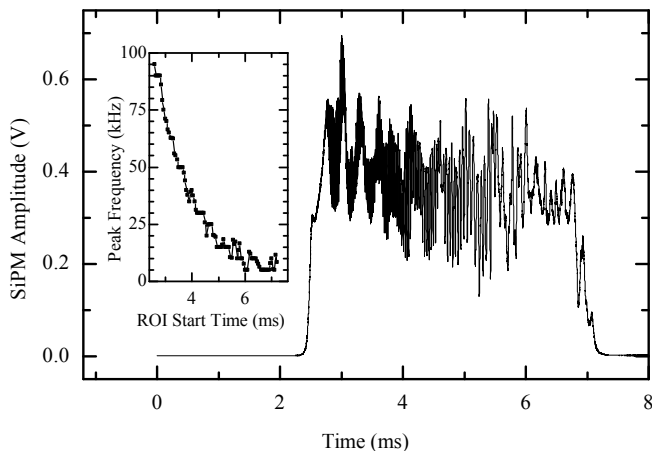


FIG. 9. Full extraction trace for a cold dense plasma with a MCP gain of ~ 2000 . Following the fast rise used for the temperature diagnostic, the slow oscillations are evidence of diocotron oscillations. The inset plots the peak FFT frequency using a rolling region-of-interest (ROI) of width 0.2 ms. These high frequencies may be related to Kelvin-Helmholtz instabilities. In accordance with the data in the inset, the frequency of such oscillations should decline as the plasma charge decreases.

however, the SNR is sufficiently high that, for most plasmas, the MCP can be run at less than its maximum gain. The gain can be set such that the MCP never saturates during the extraction process (see Fig. 9). Under these conditions, several additional plasma parameters can be measured simultaneously with the temperature measurement:

1. From the integrated SiPM signal, we can determine a number proportional to the total plasma charge.
2. For a dense, cold plasma, the plasma's self consistent potential energy is large compared to the kinetic energy of its constituents. Consequently, the first appearance of escaped electrons marks when the confinement barrier height is approximately equal to the plasma potential. Similarly, the last appearing electron marks when the confinement barrier has flattened. Thus, from the energy width of the escape curve, we can determine the plasma potential.
3. Plasma imaging²⁰ is normally done with a fast extraction lasting less than $1 \mu\text{s}$. The extractions used to measure the plasma temperature are relatively slow because we need to measure the time-history of the extraction. This leads to diocotron^{21,22} and possibly Kelvin-Helmholtz²³ instabilities that perturb the late extraction process, signs of which can be seen in Fig. 9. Nonetheless, we can image the plasma during the temperature extraction process. Even with a slow extraction, the number of plasma charges, the plasma size, and the plasma radial position can often be inferred with $\sim 10\%$ precision despite the instabilities, particularly if the plasma density is low or if the temperature is high.

V. CONCLUSION

A SiPM-based diagnostic has numerous advantages over a FC-based diagnostic for measuring the temperature of a plasma confined in a Penning-Malmberg trap. The SiPM device features enhanced robustness with low voltage operation at high speed. It permits measurements with the sensitivity of a photomultiplier tube in an environment where a photomultiplier cannot be used, and can achieve single plasma electron resolution when coupled with an MCP and phosphor screen.

Much of the advantage of a SiPM over a FC comes from the reduced noise of the SiPM-based system. It is somewhat surprising that the SiPM system, which counts electrons by converting the electrons to light, and then converting them back into electrons, is quieter than the FC system which counts electrons directly. This is particularly surprising because most of the light is lost; only ~ 0.001 sr of the light is collected by the SiPM. Some of this loss is compensated for by the gain of the phosphor screen. The efficiency of the P47 phosphors used in our screen is not well documented, but one can estimate that 10–100 photons per incident electron are generated when the screen is at 4.5 kV.²⁴ Whatever the SiPM-based system efficiency, it is high enough to produce much quieter signals than the microphonic-degraded FC system.

ACKNOWLEDGMENTS

This work was supported by the DOE OFES and NSF-DOE Program in Basic Plasma Science.

- ¹J. H. Malmberg and J. S. deGrassie, *Phys. Rev. Lett.* **35**, 577 (1975).
- ²A. W. Hyatt, C. F. Driscoll, and J. H. Malmberg, *Phys. Rev. Lett.* **59**, 2975 (1987).
- ³B. R. Beck, J. Fajans, and J. H. Malmberg, *Phys. Rev. Lett.* **68**, 317 (1992).
- ⁴J. R. Danielson and C. M. Surko, *Phys. Rev. Lett.* **94**, 035001 (2005).
- ⁵G. B. Andresen, M. D. Ashkezari, M. Baquero-Ruiz, W. Bertsche, P. D. Bowie, E. Butler, C. L. Cesar, S. Chapman, M. Charlton, A. Deller, S. Eriksson, J. Fajans, T. Friesen, M. C. Fujiwara, D. R. Gill, A. Gutierrez, J. S. Hangst, W. N. Hardy, M. E. Hayden, A. J. Humphries, R. Hydomako, S. Jonsell, N. Madsen, S. Menary, P. Nolan, A. Olin, A. Povilus, P. Pusa, F. Robicheaux, E. Sarid, D. M. Silveira, C. So, J. W. Storey, R. I. Thompson, D. P. van der Werf, J. S. Wurtele, and Y. Yamazaki (ALPHA Collaboration), *Phys. Rev. Lett.* **106**, 145001 (2011).
- ⁶A. P. Povilus, N. D. DeTal, L. T. Evans, N. Evetts, J. Fajans, W. N. Hardy, E. D. Hunter, I. Martens, F. Robicheaux, S. Shanman, C. So, X. Wang, and J. S. Wurtele, *Phys. Rev. Lett.* **117**, 175001 (2016).
- ⁷E. Sarid, F. Anderegg, and C. F. Driscoll, *Physics of Plasmas* **2**, 2895 (1995).
- ⁸E. D. Hunter, A. Christensen, J. Fajans, T. Friesen, E. Kur, and J. S. Wurtele, "Electron cyclotron resonance (ecr) magnetometry with a plasma reservoir," (2019), arXiv:1912.04358 [physics.plasm-ph].
- ⁹M. Ahmadi, B. X. R. Alves, C. J. Baker, W. Bertsche, E. Butler, A. Capra, C. Carruth, C. L. Cesar, M. Charlton, S. Cohen, R. Collister, S. Eriksson, A. Evans, N. Evetts, J. Fajans, T. Friesen, M. C. Fujiwara, D. R. Gill, A. Gutierrez, J. S. Hangst, W. N. Hardy, M. E. Hayden, C. A. Isaac, A. Ishida, M. A. Johnson, S. A. Jones, S. Jonsell, L. Kurchaninov, N. Madsen, M. Mathers, D. Maxwell, J. T. K. McKenna, S. Menary, J. M. Michan, T. Momose, J. J. Munich, P. Nolan, K. Olchanski,

- A. Olin, P. Pusa, C. . Rasmussen, F. Robicheaux, R. L. Sacramento, M. Sameed, E. Sarid, D. M. Silveira, S. Stracka, G. Stutter, C. So, T. D. Tharp, J. E. Thompson, R. I. Thompson, D. P. van der Werf, and J. S. Wurtele (ALPHA Collaboration), *Nat. Commun.* **8**, 681 (2017).
- ¹⁰D. L. Eggleston, C. F. Driscoll, B. R. Beck, A. W. Hyatt, and J. H. Malmberg, *Phys. Fluids B* **4**, 3432 (1992).
- ¹¹B. R. Beck, *Measurement of the Magnetic and Temperature Dependence of the Electron-Electron Anisotropic Temperature Relaxation Rate*, Ph.D. thesis, University of California, San Diego (1990).
- ¹²R. Hawkes, A. Lucas, J. Stevick, G. Llosa, S. Marcatili, C. Piemonte, A. D. Guerra, and T. A. Carpenter, in *2007 IEEE Nuclear Science Symposium Conference Record*, Vol. 5 (2007) pp. 3400–3403.
- ¹³P. Buzhan, B. Dolgoshein, A. Ilyin, V. Kantserov, V. Kaplin, A. Karakash, A. Pleshko, E. Popova, S. Smirnov, Y. Volkov, L. Filatov, S. Klemin, and F. Kayumov, “The advanced study of the silicon photomultiplier,” in *Advanced Technology and Particle Physics* (World Scientific, 2002) pp. 717–728.
- ¹⁴B. Godfrey, T. Anderson, E. Breedon, J. Cutter, N. Dhaliwal, O. Dalager, S. Hillbrand, M. Irving, A. Manalaysay, J. Montoya, J. Morad, C. Neher, D. Stolp, M. Tripathi, and R. Wilson, *Journal of Instrumentation* **13**, C03041 (2018).
- ¹⁵M. Stagliano, L. Abegão, A. Chiericia, and F. d’Errico, *International Journal of Science and Engineering* (2018).
- ¹⁶C. Hansen, A. B. Reimann, and J. Fajans, *Phys. Plasmas* **3**, 1820 (1996).
- ¹⁷A. J. Peurrung and J. Fajans, *Rev. Sci. Instrum.* **64**, 52 (1993).
- ¹⁸G. B. Andresen, W. Bertsche, P. D. Bowe, C. C. Bray, E. Butler, C. L. Cesar, S. Chapman, M. Charlton, J. Fajans, M. C. Fujiwara, D. R. Gill, J. S. Hangst, W. N. Hardy, R. S. Hayano, M. E. Hayden, A. J. Humphries, R. Hydomako, L. V. Jørgensen, S. J. Kerrigan, L. Kurchaninov, R. Lambo, N. Madsen, P. Nolan, K. Olchanski, A. Olin, A. P. Povilus, P. Pusa, E. Sarid, S. Seif El Nasr, D. M. Silveira, J. W. Storey, R. I. Thompson, D. P. van der Werf, and Y. Yamazaki (ALPHA Collaboration), *Rev. Sci. Instrum.* **80**, 123701 (2009).
- ¹⁹M. E. Glinsky, T. M. O’Neil, M. N. Rosenbluth, K. Tsuruta, and S. Ichimaru, *Phys. Fluids B* **4**, 1156 (1992).
- ²⁰A. P. Povilus, *Cyclotron-cavity mode resonant cooling in single component electron plasmas*, Ph.D. thesis, University of California, Berkeley (2015).
- ²¹R. H. Levy, *Phys. Fluids* **8**, 1288 (1965).
- ²²K. S. Fine and C. F. Driscoll, *Phys. Plasmas* **5**, 601 (1998).
- ²³A. J. Peurrung and J. Fajans, *Phys. Fluids A* **5**, 493 (1993).
- ²⁴P. Hoess and K. Fleder, in *24th International Congress on High-Speed Photography and Photonics*, Vol. 4183 (International Society for Optics and Photonics, 2001) pp. 127–132.